Experimental Eye Research 219 (2022) 109033

Contents lists available at ScienceDirect

Experimental Eye Research

journal homepage: www.elsevier.com/locate/yexer

Short communication

Evidence for endogenous exchange of cytoplasmic material between a subset of cone and rod photoreceptors within the adult mammalian retina via direct cell-cell connections

Patrick Heisterkamp [a,1], Oliver Borsch [a,1], Nundehui Diaz Lezama [a], Sylvia Gasparini [a], Adeeba Fathima [b], Livia S. Carvalho [c], Felix Wagner [a,d], Mike O. Karl [a,d], Michael Schlierf [b], Marius Ader [a,*]

[a] CRTD/Center for Regenerative Therapies Dresden, Center for Molecular and Cellular Bioengineering, Technische Universität Dresden, 01307, Dresden, Germany
[b] B CUBE/Center for Molecular and Cellular Bioengineering, Technische Universität Dresden, 01307, Dresden, Germany
[c] Center for Ophthalmology and Visual Sciences Incorporating the Lions Eye Institute, The University of Western Australia, Nedlands, Nedlands, 6009, Western Australia, Australia
[d] German Center for Neurodegenerative Diseases (DZNE) Dresden, 01307, Dresden, Germany

ARTICLE INFO

Keywords:
Photoreceptor
Cone
Rod
Material transfer
STORM
Cell-cell connection

ABSTRACT

Photoreceptor cell transplantation into the mouse retina has been shown to result in the transfer of cytoplasmic material between donor and host photoreceptors. Recently it has been found that this inter-photoreceptor material transfer process is likely to be mediated by nanotube-like structures connecting donor and host photoreceptors. By leveraging cone-specific reporter mice and super-resolution microscopy we provide evidence for the transfer of cytoplasmic material also from endogenous cones to endogenous rod photoreceptors and the existence of nanotube-like cell-cell connections possibly mediating this process in the adult mouse retina, together with preliminary data indicating that horizontal material transfer may also occur in the human retina.

It has recently been shown that transplantation of photoreceptors rescues some visual function in mouse models of retinal degeneration (Santos-Ferreira et al., 2015; Pearson et al., 2012). These improvements in vision, however, do not appear to be a result of structural integration of donor photoreceptors into the host retina, when endogenous but dysfunctional photoreceptors remain, but rather from the exchange of cytoplasmic material (e.g. proteins, RNA or organelles) between donor and host photoreceptors (Pearson et al., 2016; Santos-Ferreira et al., 2016; Singh et al., 2016).

Recently, two back-to-back published studies by Ortin-Martinez et al. (2021) and Kalargyrou et al. (2021) presented evidence that nanotube-like connections between donor and host photoreceptors underlie this transfer of cytoplasmic material. These interconnecting tubules have been termed photoreceptor nanotubes (^{Ph}NTs) and were found to mediate the exchange of cytoplasmic components, lipid-bound materials, and organelles *in vitro* as well as *in vivo* in transplantation settings. It is currently unclear whether this nanotube-mediated transfer is accomplished through passive diffusion and/or a motor protein-driven transport through truly "open-ended" connections (Henderson and Zurzolo, 2021). Additionally, Kalargyrou et al. indicated the possibility of material transfer also between endogenous rod photoreceptors by using chimeric mice with either Cre-expressing or floxed fluorescence reporter-gene harbouring photoreceptor cells. Detection of fluorescent cells were indicative for successful horizontal Cre-transfer between endogenous photoreceptors. However, it is still unclear whether horizontal material transfer (i) is mediated by ^{Ph}NTs, (ii) appears during retinal development or persists during adulthood, given permanent expression of fluorescent reporters following a single Cre recombinase event, and (iii) is mediated between specific photoreceptor subtypes, i.e. rods or cones.

Here, we investigated photoreceptor material transfer between endogenous photoreceptors through the use of two transgenic mouse lines that exclusively express GFP in cones. We observed GFP-positive rods indicative of a steady-state transfer of reporter mRNA or protein from cones to rods in the adult retina.

For this purpose, we used (i) OPN1-GFP mice that contain a

* Corresponding author. CRTD/Center for Regenerative Therapies Dresden, Technische Universität Dresden, Fetscherstrasse 105, 01307, Dresden, Germany.
E-mail address: marius.ader@tu-dresden.de (M. Ader).
[1] Equal contribution.

https://doi.org/10.1016/j.exer.2022.109033
Received 6 December 2021; Received in revised form 8 March 2022; Accepted 8 March 2022
Available online 11 March 2022

transgene composed of a 6.8 kb regulatory sequence 5′ of the human red and green opsin gene driving GFP expression (Fei and Hughes, 2001), and (ii) Chrnb4-GFP mice, in which the enhanced GFP (EGFP) gene was inserted upstream of the cholinergic receptor nicotinic beta 4 subunit (Chrnb4) gene (Siegert et al., 2009; Brunet et al., 2020).

All experiments were carried out on adult animals (6–14 weeks) of both sexes. The experiments were approved by the Landesdirektion Dresden (approval no.: TVA 10/2018; DD24.1–513/450/0). Animal experiments were conducted in accordance with the regulations from the European Union, German laws (Tierschutzgesetz), the ARVO Statement for the Use of Animals in Ophthalmic and Vision Research, and the NIH Guide for the care and use of laboratory animals. All used animals were bred and housed by the animal facility of the Center for Regenerative Therapies Dresden, Technische Universität Dresden.

To obtain retinal samples, experimental animals were sacrificed via anaesthetic overdose. Eyes were enucleated and fixed in 4% (wt/vol) paraformaldehyde (PFA) in PBS for 1 h at 4 °C. Cornea and lens were removed and the remaining parts of the eye (sclera, choroid, retina) were cryoprotected in 30% (wt/vol) sucrose in PBS overnight at 4 °C. Eyes were cryo-embedded and serial transverse cryosections of mouse retinas were prepared at 20 μm thickness unless indicated otherwise. Sections were air-dried for 15 min, at 37 °C.

For immunohistochemistry, samples were rehydrated with PBS for 30 min and incubated with blocking solution, consisting of 0.3% (vol/vol) Triton-X100, 1% (wt/vol) BSA, and 5% (vol/vol) goat serum in PBS for 1 h at room temperature. Samples were incubated with primary antibodies in 1% (wt/vol) BSA in PBS overnight at 4 °C. Primary antibodies used were anti-cone arrestin (1:2500; Cat#ab15282, Merck Millipore), anti-GFP (1:500; Cat#ab13970, Abcam) and anti-Nr2e3 (1:800; Cat#PP-H7223–00, R&D systems) for mouse sections and anti-cone arrestin antibody 7G6 (1:100; kind gift of Prof. Wolfgang Baehr, University of Utah) for human sections. After three washes with PBS, incubation with secondary antibodies and DAPI (1:15000) in PBS was performed for 1 h 30 min at RT. Secondary antibodies used were (all from Jackson IR): Alexa Fluor 488 goat anti-chicken IgG (1:1000; Cat#103-545-155, Merck KGaA), Cy3 goat anti-rabbit IgG (1:1000; Cat#111-165-144, Merck KGaA), Cy5 goat anti-mouse IgG (1:1000; Cat#115-175-146, Merck KGaA). Samples were washed three times with PBS and mounted using Aqua-Poly/Mount (Cat#18606-20, Polysciences Inc.). Immunostainings were imaged using a structured illumination microscopy (Zeiss Axio Imager.Z2 with Apotome module, Carl Zeiss, Germany) and the software Zeiss Zen blue 2.6. Images were processed offline using Zeiss Zen blue 2.6, Fiji image processing, and Inkscape 0.92. Total numbers of GFP^+ rods within mouse retinas were quantified by counting reporter positive cells on every 4th serial cryosection of a whole mouse eye and multiplying this value by 4 to arrive at a whole eye estimate. Rods were differentiated from cones by their lack of strong cone arrestin expression, their positivity for Nr2e3, and their unique (inverted) nuclear morphology (Solovei et al., 2009). In addition, since cone perikarya tend to be located at the outer edge of the ONL, only rods at least 3 cell layers from the ONL edge were counted.

When assessing sectioned retinal tissue from adult OPN1-GFP or Chrnb4-GFP animals, we observed GFP^+ cells in the outer nuclear layer (ONL) that morphologically resembled rod photoreceptors (Fig. 1a). In contrast to cone cell bodies which expressed high levels of GFP and are exclusively located at the apical side of the ONL, these cells were located deeper within the ONL and displayed a rod-like, i.e. round, cell body and generally lower levels of GFP intensity suggesting that these cells represent rods that have taken up GFP from nearby GFP-expressing cones (Fig. 1b). We confirmed the rod-identity of these dimly GFP^+ cells by immunohistochemical staining, since these cells expressed the rod-specific nuclear marker Nr2e3 (Fig. 1c and d), and their DAPI-stained nuclei possess a single, dense heterochromatin center (Fig. 1c'', d'') characteristic of the inverted nuclear architecture of rods in nocturnal animals (Fig. 1b). This stands in contrast with cones that display several small dispersed heterochromatin centers (Fig. 1c', d') (Solovei et al., 2009).

Quantification of cone-GFP retinas revealed an average of around 1479 (Chrnb4-GFP) to 1820 (OPN1-GFP) GFP^+ rods per retina (Fig. 1e). However, the number of cones and rods truly engaging in horizontal material transfer might be underestimated since GFP expression in the OPN1-GFP retina shows a heterogeneous ventral to dorsal reporter expression (Fei and Hughes, 2001), limited to 9% of cones in the ventral retinal region and up to 50% in the dorsal region (Lipinski et al., 2011). Similarly, in Chrnb4-GFP retinas only about 5% of cones are reporter-labelled in pigmented mice (Brunet et al., 2020), hence the number of material-receiving rods could be by more than a magnitude higher than reported here.

To elucidate whether GFP protein or mRNA is transferred from cones to rods we used Stellaris® single-molecule RNA-FISH. We analysed 5 μm thin retinal cryosections with probes recognizing GFP mRNA, labelled with Quasar® 570 (catalogue no. VSMF-1014-5, LGC Biosearch Technologies) following the manufacturer's instructions for frozen tissue. While GFP protein, i.e. GFP fluorescent signal, was identified in a subset of rods in both cone-specific reporter mouse lines, we did not observe any traces of GFP mRNA within GFP^+ rods whereas it was abundantly present in GFP^+ cones (Fig. 1f). This suggests that GFP^+ rods do not contain transferred mRNA nor express GFP mRNA themselves. This finding implies that protein, rather than mRNA, is transferred from cones to rods and that leaky reporter gene expression is unlikely to cause the observed GFP positivity in rods. In addition, we also observed GFP^+ rods deep within the ONL in unfixed, whole live retinas, thereby ruling out the possibility of a tissue processing artefact leading to rod GFP positivity (Fig. 1g).

In retinal sections we frequently observed that the cell bodies of GFP^+ rods were located directly adjacent to axons of GFP-expressing cones (e.g. Fig. 1a). Hence, we hypothesized a causal relationship between GFP-positivity of rods and proximity to GFP^+ cone axons.

The three-dimensional relationship between photoreceptors can only be partially analysed in sections, as any structural information outside the plane of sectioning may be lost. Thus, we analysed the relationship between GFP^+ rods and cones in OPN1-GFP retinas in retinal wholemounts.

To prepare retinal wholemounts, enucleated eyes were punctured through the cornea using a 30 gauge needle, and fixed initially with 4% PFA in PBS for 20 min at 4 °C. After fixation eyes were dissected to extract the retina. Using a Pasteur pipet with cut tip, the isolated retina was transferred on top of 0.4 μm Millicell® culture inlays (Cat#-PICM03050, MerckKGaA) and placed within 6-well plates. Excess PBS around the retina was removed and 1 ml 4% PFA in PBS was added to the lower compartment into the well for further fixation for 20 min, at room temperature, while on a shaker. After incubation, an additional 2 ml of 4% PFA was added on top of the inlay for further fixation for 20 min, at room temperature, shaking. After incubation, PFA was exchanged with PBS and retinas were transferred to a 24-well plate and washed twice with PBS for 15 min, at room temperature, shaking. Samples were incubated in 1 ml blocking buffer, consisting of 0.3% Triton X-100, 1% BSA, and 5% goat serum in PBS, for 2 h, at room temperature, shaking. Blocking buffer was discarded and samples were incubated with 1 ml primary antibody in 0.3% Triton-X100, 1% BSA in PBS for 3 days, at 4 °C, shaking. The sample was washed three times with PBS for 15 min, at 4 °C. Incubation with secondary antibody in 0.3% Triton-X100, 1% FBS, and DAPI in PBS was performed overnight, at 4 °C, shaking. The sample was washed three times in PBS for 30 min, at 4 °C, shaking. The retina was then mounted in Aqua-Poly/Mount with the photoreceptor side facing the coverslip. Retinal wholemounts were imaged using a spinning disk microscope (Andor Dragonfly, Oxford Instruments) with Andor Fusion 2.0, or a laser-scanning confocal microscope (LSM780 upright, Carl Zeiss) with Airyscan2 super-resolution detector and Zeiss Zen black 2.1. Distances between the cell bodies of GFP^+ rods and axons of GFP^+ cones were analysed through distance-measurement within a 332.8 μm × 332.8 μm square retinal stack

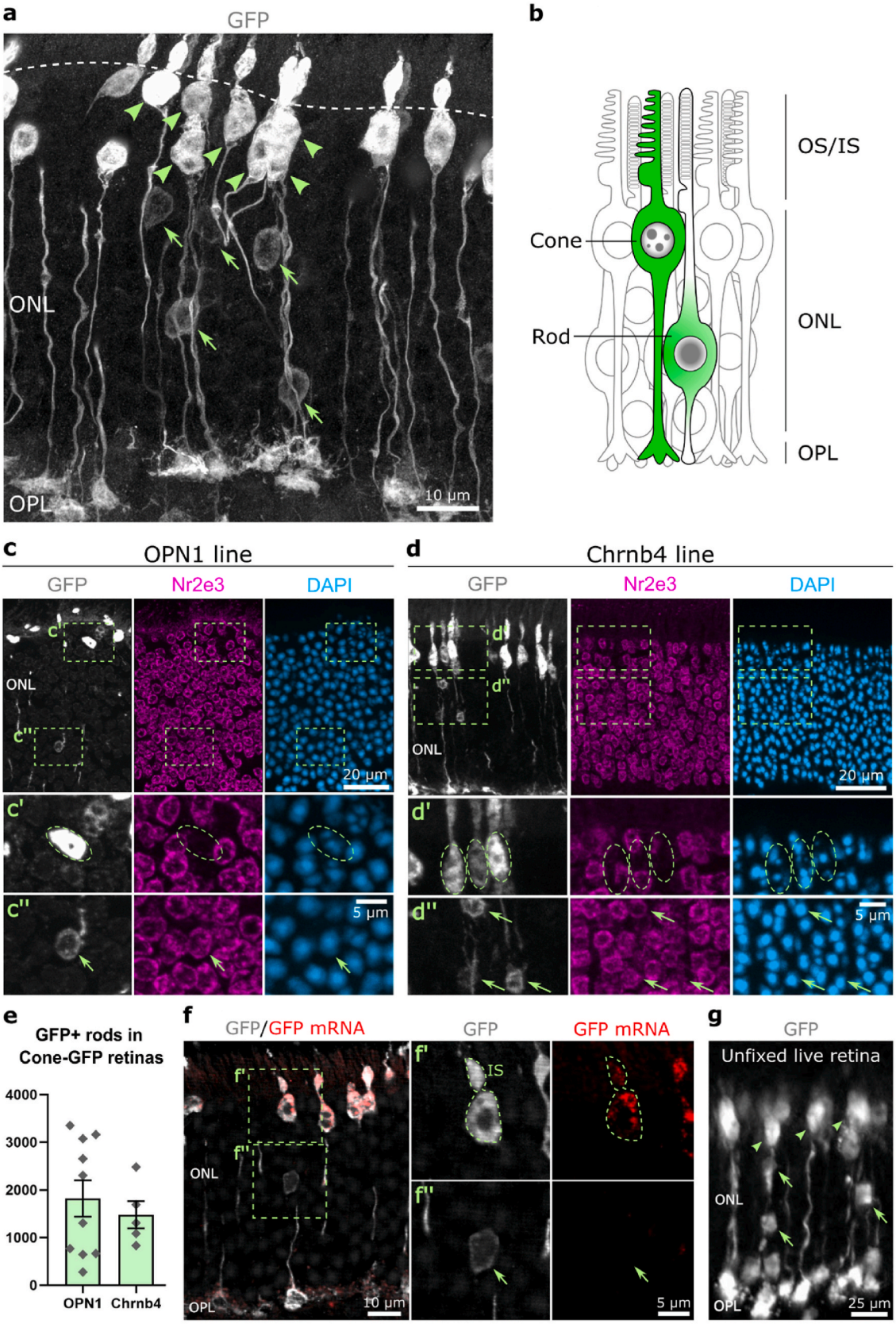

(caption on next page)

Fig. 1. Presence of reporter-positive rod photoreceptors in the retinas of cone photoreceptor reporter mouse lines. **a**: The outer nuclear layer (ONL) of OPN1-GFP retinas contains strongly fluorescent cone photoreceptors (arrowheads) in the typical location in the outer (apical) region of the ONL (below dashed line) and unexpected dim GFP$^+$ cell bodies (arrows) in deeper ONL-regions, atypical for cone photoreceptors. **b**: Illustration depicting the presence of GFP$^+$ cones and rods in GFP cone photoreceptor reporter lines distinguished by divergent nuclear architecture and localization within the ONL. Lower GFP levels in rods (green colour fading) might be caused by intracellular diffusion effects of GFP following cone to rod transfer. **c/d**: GFP$^+$ photoreceptor location, rod-marker expression, and nuclear architecture confirm rod identity of dim GFP$^+$ cells in OPN1-GFP and Chrnb4-GFP cone reporter mouse lines. Bright GFP$^+$ cone cell bodies (c'/d') are located exclusively at the apical edge of the ONL and lack the rod marker Nr2e3. Additionally, cone nuclei display the typical nuclear architecture with several small dispersed chromocenters (c'/d'). The more basally located dim GFP$^+$ cells are positive for the rod-specific marker Nr2e3 and display no dispersed chromocenters, but instead one single heterochromatin center (inverted nuclear architecture) typical for rods of nocturnal animals (c''/d''). **e**: Quantification of GFP$^+$ rods in OPN1-GFP and Chrnb4-GFP mice. 1820 ± 362 GFP$^+$ rods per OPN1-GFP retina (mean ± SEM; n = 10) and 1479 ± 287 GFP$^+$ rods per Chrnb4-GFP retina (mean ± SEM; n = 5). **f**: Single-molecule RNA-FISH reveals GFP mRNA in cell bodies and inner segments of GFP$^+$ cones (e') but is undetectable in GFP$^+$ rods (e''). IS = inner segment. **g:** Reporter positive cones (arrowheads) at apical edge of ONL and reporter positive rods (arrows) deep within ONL of an unfixed live OPN1-GFP retina. ONL = outer nuclear layer. OPL = outer plexiform layer. (For interpretation of the references to colour in this figure legend, the reader is referred to the Web version of this article.)

using FIJI image processing. To this end, the smallest horizontal distance between GFP$^+$ rod cell bodies and the closest nearby GFP$^+$ cone axon was assessed (Fig. 2a).

Analysis of retinal wholemounts through spinning disk microscopy confirmed that in the vast majority of cases the cell bodies of GFP$^+$ rods are located close to the axons of GFP$^+$ cones (Fig. 2b). Importantly, quantification of the distance between the cell bodies of GFP$^+$ rods and GFP$^+$ cone axons in OPN1-GFP retinas revealed an average distance of only 1.1 ± 0.3 μm (mean ± SEM; Fig. 2b'), which is significantly lower than the distance that would be expected given a random distribution of rods in relation to cones (ca. 4.24 μm; assuming equidistant distribution of 358 cones in a 332.8 μm × 332.8 μm retinal square stack, Fig. 2a).

Intriguingly, during analysis we noticed that particularly GFP$^+$ rods would occasionally display a faint cone-arrestin signal, which is known to be a cone-specific marker. Therefore, we asked if this phenomenon could be leveraged to analyse whether horizontal material transfer between photoreceptors also exists in wild-type mice and human retinas.

Human retinal tissue samples were obtained from subjects that have given their informed consent for the use of their biological material for research purposes. The study was conducted in accordance with the Declaration of Helsinki. The protocol was approved by the Ethics Committee of TU Dresden, Dresden, Germany (EK 322082017).

Analysis of retinal sections from wild-type mice did indeed reveal rare, but distinct cases of rod cell bodies expressing cArr, i.e. cells expressing Nr2e3 and having inverted nuclei, but containing low levels of cArr (Fig. 2c). Furthermore, analysis of human retinal tissue also revealed occasional rods faintly positive for cArr (Fig. 2d) (anti-cone arrestin antibody 7G6; 1:100; gift of Prof. Wolfgang Baehr, University of Utah). While antibody cross-reactivity could be argued to underlie the few instances of faint cArr + rods, the singular presence of such rods close to cone axons closely resembles the horizontal material transfer pattern of GFP$^+$ rods observed in the analysed cone-GFP reporter lines. Moreover, in case of a nonspecific cArr antibody binding in rods, it could be assumed that not only few but many rods within the stained ONL would be found to be faintly cArr positive. These observations indicate the possibility that horizontal material transfer also occurs in wild-type mouse and human retinas, and thus might represent a general feature of photoreceptor-photoreceptor interactions in adult mammals.

Intriguingly, we found indications for thin protrusions formed between cell bodies of GFP$^+$ rods and GFP$^+$ cone axons within retinal sections and wholemounts (Fig. 2e and f) pointing to potential direct cell-cell connections as the underlying mechanism of GFP transfer. However, these potential connections remained partly elusive due to the resolution limitations of conventional light microscopy of about 200 nm. To circumvent this barrier, we made use of STORM super-resolution microscopy that can achieve resolutions down to 20 nm (Rust et al., 2006). We utilized STORM on retinal cryosections to pinpoint potential cone-to-rod connections. To prepare samples for STORM, retinas were fixed and isolated as described above. After initial incubation with PFA, retinas were carefully cut into four parts of equal size before being transferred to Millicell® culture inlays placed in a 6-well plate. Fixation was continued by adding 4% PFA in PBS into the compartment below the inlay for 20min, at room temperature, while on a shaker. Afterwards, additional 2 ml of 4% PFA were added on top of the inlay for further fixation of the retina for 20 min, at room temperature, shaking. The samples were washed two times with PBS, for 15 min each, at room temperature, shaking. Retinas were then cryoprotected in 20% (wt/vol) sucrose in PBS for 1 h at 4 °C, and 30% (wt/vol) sucrose in PBS for 1 h at 4 °C. The 4 retinal sections, including underlying membrane were cut out and stacked on top of each other in small cryomolds (10 × 10 × 5 mm), filled with NEG-50, and frozen. Cryosections were prepared at 12 μm thickness and 4 cryosections each taken up on a #1.5 Poly-L-Lysine coated coverslip. Samples were dried at 37 °C for 15 min before being stored at 4 °C, to prevent additional freeze-thaw-cycles, until further processing (typically the next day). Regions-of-interest were preselected by reversibly mounting the coverslips in PBS-filled moulds of a 0.12 mm spacer (SecureSeal™, Grace Bio-Labs) attached to a glass slide and imaged using widefield fluorescence microscopy. After ROIs had been selected, the respective samples were stained using anti-GFP nanobodies (Cat# gt-250, Chromotek) (Ries et al., 2012) conjugated to AlexaFluor 647 (Cat#10769744, Fisher Scientific). Briefly, samples were washed three times with PBS and permeabilized via incubation in 0.5% Triton X-100 (vol/vol) in PBS for 15 min at room temperature. Slides were washed twice with PBS and blocked using 4% (wt/vol) BSA in PBS for 1 h at room temperature. Samples were incubated with anti-GFP nanobodies in blocking buffer for 1 h at room temperature, followed by washing twice with PBS and incubation with DAPI in PBS for 10 min. Samples were then quickly rinsed with dH_20 and mounted in activation buffer. Activation buffer for Alexa Fluor 647 blinking consisted of 100 mM cysteamine hydrochloride (M6500, Sigma Aldrich), 1% (wt/vol) d-glucose, 5 kU/ml catalase (E3289, Sigma-Aldrich) and 5 mg/ml pyranose oxidase (P4234, Sigma-Aldrich (Swoboda et al., 2012) in PBS at pH 7.4, and was prepared immediately prior to mounting during the DAPI staining step. Samples were mounted in 20 μl of activation buffer on Starfrost® Advanced Adhesive Slides with 0.12 mm spacer and imaged within 2 h after sample preparation. Overview images of these samples were taken using a Nikon Ti-E microscope with Andor iXON-Ultra 888 EMCCD camera. STORM imaging was performed on a NIKON N-STORM TIRF (Nikon, Japan) setup using a 100x oil objective with NA 1.49. Alexa Fluor 647 dye molecules, conjugated to anti-GFP nanobodies, were excited with 50 mW end of fiber 647 nm laser and activated by increasing the power of a 405 nm laser from 0.1 to 1 mW. 20.000 frames with an exposure time of 20 ms were acquired. Image acquisition was done with an Andor iXon 897 Ultra (Oxford Instruments, Belfast, UK) EMCCD camera. The STORM image was reconstructed using the ThunderSTORM ImageJ plug-in (Ovesný et al., 2014). Raw image stacks comprising 20,000 images were corrected for lateral drift using the built-in cross-correlation based method. We chose a wavelet filter (order 3, scale 2) for localization detection. Sub-pixel localization is achieved by a 2D integrated Gaussian fit to the point spread function. We determined the average localization uncertainty as 20 nm.

STORM imaging revealed the presence of GFP$^+$ tubule-like

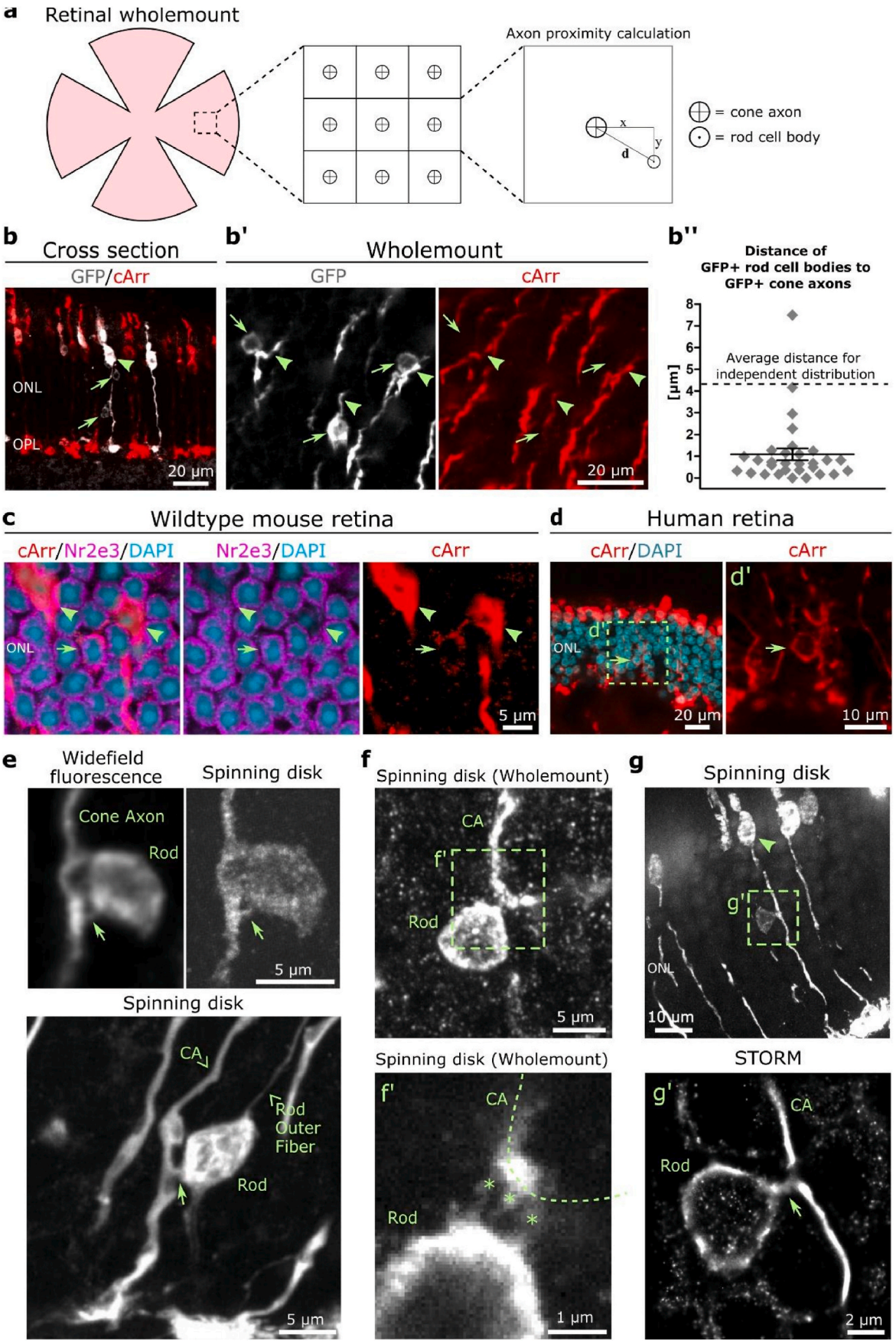

(caption on next page)

Fig. 2. Direct cell-cell connections may mediate horizontal material transfer between cones and rods in mice and humans. **a**: Illustration depicting the analysis of the spatial relationship between GFP^+ cone axons and GFP^+ rod cell bodies in retinal wholemounts analysed by optical sections. Assuming an equidistant and independent distribution of rods and cones, the expected average distance (d) between a GFP^+ rod (⊙) and the next nearby GFP^+ cone axon (⊕) would be 4.24 μm (dashed line in b''). **b**: Close proximity of GFP^+ cones and GFP^+ rods in histological cross section in the OPN1-GFP cone line. b': Microscopic analysis along optical section z-stack of retinal wholemounts confirmed that dim GFP^+ rod cell bodies (arrows) can be found almost exclusively adjacent to GFP^+ cone axons ($cArr^+$, arrowhead) and not randomly among all cone axons ($cArr^+$ only). Shown is a single optical plane derived from within the ONL of an OPN1-GFP retinal wholemount. b'': Quantification of the retinal planes within a 332.8 μm × 332.8 μm area of an OPN1-GFP wholemount (b') reveals an average distance of 1.1 ± 0.3 μm (mean ± SEM) between $GFP^+/cArr^+$ cone axons and $GFP^+/cArr^-$ rod cell bodies. This value is significantly lower than the computationally estimated distance of 4.24 μm (dashed line) given independent distribution of GFP^+ rods and cones. **c**: Indications for occasional horizontal material transfer in the wildtype mouse retina. In rare cases co-labelling of rod cell bodies (arrow; $Nr2e3^+$ and inverted nuclear architecture) with the cone-specific marker cone-Arrestin (cArr) could be observed in close vicinity to $cArr^+$ cones that lack these rod-specific nuclear markers (arrowheads). **d**: Indication for horizontal material transfer in human retinas by occasional presence of cone specific cArr in rods, identified by their deep localization within the ONL (arrow). **e**: Presence of tubule-like structural connections (arrows) between GFP^+ cone axons (CA) and rod cell bodies in retinal cross sections presumably mediating horizontal material transfer. **f**: Spinning disk imaging example (maximum intensity projection) of retinal wholemount showing the presence of nanotube-like structures (*) in a single plain analysis between GFP^+ cone axons and GFP^+ rod cell bodies. **g**: STORM super-resolution imaging of retinal cryosections confirms the presence of structural connections between a subset of cone axons and rod cell bodies. Spinning disk: Shown is a Maximum intensity projection through a 12 μm thick retinal section. A GFP^+ rod cell body (dashed box) can be seen directly adjacent to the axon of a proximate GFP^+ cone photoreceptor (arrowhead). STORM: STORM super-resolution imaging of the same sample reveals a direct tubular connection (arrow) between cone axon and rod cell body. The nanotube-like structure is ca. 1 μm long and 0.6 μm wide.

connections between rod cell bodies and cone axons in OPN1-GFP retinas (Fig. 2g). These observed structures were approximately 1 μm in length and 0.6 μm in width and may represent same or similar nanotube-like connections described by Ortin-Martinez et al. (2021) and Kalargyrou et al. (2021), both of which describe nanotubes ~0.7 μm in width. These observations represent, to our knowledge, the first recorded instances of presumably nanotube-like connections between photoreceptors in the adult mammalian retina (i.e. in the absence of photoreceptor transplantation).

The possibility of leaky expression of the reporter transgene might be argued as a reason for the presence of the observed GFP^+ rods, however together, our findings presented here point towards a genuine transfer of cytoplasmic material between adult cells. First, we directly addressed leaky reporter expression via fluorescence in situ hybridization against GFP mRNA. GFP mRNA was abundant in GFP^+ cones, however we did not detect any GFP transcripts in GFP^+ rods indicating absence of leaky transcription (Fig. 1f). Second, GFP^+ rods were identified in two independent cone-reporter mouse lines driven by different promoters (OPN1-GFP and Chrnb4-GFP) and additional examples can be found upon close inspection of figures in other published studies (e.g. Decembrini et al., 2017; Brunet et al., 2020). Furthermore, leaky expression would occur in GFP^+ rods in a distribution independent from GFP^+ cones, while our analysis demonstrates close proximity between GFP^+ cone axons and rod cell bodies. Third, the observed wildtype retinas with faint cArr-positive cells deep within the ONL and rod nuclear architecture also point to a mechanism other than leaky reporter gene expression. Moreover, direct cytoplasmic connections are observed by STORM, that resemble the recently identified photoreceptor nanotubes that mediate material transfer between donor and host photoreceptors *in vitro* and in transplantation settings (Kalargyrou et al., 2021; Ortin-Martinez et al., 2021).

While the chimera produced in the recent work by Kalargyrou et al. is intriguing, this does not exclude the possibility of Cre recombination during retinal development. Definitive proof of horizontal transfer in the adult retina could include the generation of chimeric mice between inducible e.g. Tet-on Cre recombinase mice and floxed reporter mice where Cre expression is only induced in adulthood. Regardless, in line with previous studies and through our direct observations via means of STORM, the existence of potential connections that mediate horizontal material transfer between photoreceptors seems likely.

The precise nature of these presumable ^{ph}NTs remains to be elucidated, yet they likely present a type of tunnelling nanotube (TNT). TNTs have been shown to enable material transfer between cells both *in vitro* and *in vivo* (Vignais et al., 2017), e.g. between dendritic cells in the mouse cornea, and are highly heterogenous in size, ranging from a thickness of 50 nm to 1.5 μm (Austefjord et al., 2014). The recently described nanotube-like structures mediating the material transfer between donor and host photoreceptors have been reported to be in a diameter range of about 0.7 μm (Kalargyrou et al., 2021; Ortin-Martinez et al., 2021) which is in accordance with the structural connections between endogenous photoreceptors we report in this study (ca. 0.6 μm, see Fig. 2c).

It is known that photoreceptors are extensively coupled electrically by ion exchange through gap junctions (Fain and Sampath, 2018), often via small extrusions at the axon terminals named telodendria (O'Brien et al., 2012). However, such transcellular exchange is limited to molecules <1 kDa (Bloomfield and Völgyi, 2009), a size far smaller than the transferred macromolecules observed in this study such as GFP (27 kDa) or cArr (48 kDa). The extent of biomacromolecule exchange and its biological significance remains to be explored in further studies. Additionally, although the transfer of cytoplasmic material via nanotube-like structures between donor and host photoreceptors has been shown (Kalargyrou et al., 2021; Ortin-Martinez et al., 2021), it has yet to be investigated whether the structural connections shown here are specific for cone-rod interactions or whether endogenous rod-rod or cone-cone connections also exist. Interestingly, reanalysis of single-cell RNA sequencing data from whole mouse retinas revealed the presence of a subset of cells which co-express the cone-specific gene Opn1sw and the rod-specific gene Nr2e3 (Clark et al., 2019). It is hypothesized that a transition from rod to cone fate underlies the presence of such hybrid photoreceptor populations. Alternatively, cell dissociation procedures leading to the presence of potentially RNA-filled subcellular structures in cell suspensions prior to single-cell sorting are speculated to contribute to subsequent RNA impurities (Fadl et al., 2020). It remains to be seen whether such cone and rod markers expressing 'hybrid'--photoreceptors in the developing retina and our observed horizontal transfer of material in the adult animal may represent related or independent mechanisms. In our study, we do not observe GFP-mRNA in GFP^+ rods and only few GFP^+ rods show faint cArr immuno-staining, while GFP^+ rod cell bodies are closely neighbouring GFP^+ cone axons forming nanotube-like structures between them, all strongly arguing against hybrid cells being the underlying cause. Indeed, our finding of potential protein transfer via nanotube-like structures are in line with recent transplantation studies that show no (Kalargyrou et al., 2021) or minimal amounts (Ortin-Martinez et al., 2021) of reporter mRNA in acceptor cells.

Still, the question remains what physiological purpose this exchange of material between endogenous photoreceptors might serve. Horizontal material transfer of cytoplasmic material between donor and host photoreceptors after transplantation into mouse models of inherited retinal degeneration has been hypothesized to improve vision by support of the host photoreceptors with donor-derived molecules (Gasparini et al., 2019; Nickerson et al., 2018). Hence, horizontal exchange of cytoplasmic material could pose a thus far undiscovered mechanism for

photoreceptor functional modulation and/or support in physiological or pathological conditions. Interestingly, recent studies demonstrate much closer functional interactions between rods and cones than previously thought (Münch et al., 2009; Szikra et al., 2014). Thus, deciphering the nature, extent and directionality of transferred cytoplasmic material between mammalian photoreceptors may help to gain further insights into the complex interactions within the retina.

Author contributions

O.B., P.H., S.G., and M.A. conceived this study. O.B., P.H., S.G., M.S., and M.A. designed the experiments. O.B., P.H., N.D-L., and L.C. prepared the samples with assistance from A.F.; O.B., P.H., F.W. and N.D-L. carried out imaging and O.B., P.H., N.D-L. and A.F. performed image analysis. P.H. performed the computational analysis. O.B., P.H., S.G., and M.A. wrote this paper with input from all authors. O.B. and P.H. contributed equally.

Declaration of competing interest

The authors declare no competing interests.

Acknowledgements

This work was supported by the Molecular Imaging and Manipulation Facility with help from Jens Ehrig, and the Light-Microscopy Facility (LMF) with the help of Ali Gheisari, core facilities of the CMCB at Technische Universität Dresden. We thank Dierk Wittig and Mike O. Karl for the provision of human tissue samples and Paula Fuller-Carter and Annie Miller for preparation of retinal samples and shipment organisation. This work was financially supported by the Deutsche Forschungsgemeinschaft (DFG): AD375/6-1, FZT 111 Center for Regenerative Therapies Dresden, and EXC68. Supported by the Funding Programs for DZNE Helmholtz (M.K.); TU Dresden CRTD (M.K.); and DFG KA2794/5-1 SPP2127 (F.W., M.K.).

References

Austefjord, M.W., Gerdes, H.-H., Wang, X., 2014. Tunneling nanotubes. Commun. Integr. Biol. 7, e27934.
Bloomfield, S.A., Völgyi, B., 2009. The diverse functional roles and regulation of neuronal gap junctions in the retina. Nat. Rev. Neurosci. 10, 495–506.
Brunet, A.A., Fuller-Carter, P.I., Miller, A.L., Voigt, V., Vasiliou, S., Rashwan, R., Hunt, D. M., Carvalho, L.S., 2020. Validating fluorescent Chrnb4.EGFP mouse models for the study of cone photoreceptor degeneration. Transl. Vis. Sci. Technol. 9, 28.
Clark, B.S., Stein-O'Brien, G.L., Shiau, F., Cannon, G.H., Davis-Marcisak, E., Sherman, T., Santiago, C.P., Hoang, T.V., Rajaii, F., James-Esposito, R.E., et al., 2019. Single-cell RNA-seq analysis of retinal development identifies NFI factors as regulating mitotic exit and late-born cell specification. Neuron 102, 1111–1126 e5.
Decembrini, S., Martin, C., Sennlaub, F., Chemtop, S., Biel, M., Samardzija, M., Moulin, A., Behar-Cohen, F., Arsenijevic, Y., 2017. Cone genesis tracing by the Chrnb4-EGFP mouse line: evidences of cellular material fusion after cone precursor transplantation. Mol. Ther. 25 (3), 634–653.
Fadl, B.R., Brodie, S.A., Malasky, M., Boland, J.F., Kelly, M.C., Kelley, M.W., Boger, E., Fariss, R., Swaroop, A., Campello, L., 2020. An optimized protocol for retina single-cell RNA sequencing. Mol. Vis. 26, 705–717.
Fain, G., Sampath, A.P., 2018. Rod and cone interactions in the retina. F1000Res. 7.
Fei, Y., Hughes, T.E., 2001. Transgenic expression of the jellyfish green fluorescent protein in the cone photoreceptors of the mouse. Vis. Neurosci. 18, 615–623.
Gasparini, S.J., Llonch, S., Borsch, O., Ader, M., 2019. Transplantation of photoreceptors into the degenerative retina: current state and future perspectives. Prog. Retin. Eye Res. 69, 1–37.
Henderson, J.M., Zurzolo, C., 2021. Seeing eye to eye: photoreceptors employ nanotube-like connections for material transfer. EMBO J 40 (22), e109727, 2021 Nov 15.
Kalargyrou, A.A., Basche, M., Hare, A., West, E.L., Smith, A.J., Ali, R.R., Pearson, R.A., 2021. Nanotube-like processes facilitate material transfer between photoreceptors. EMBO Rep 22 (11), e53732, 2021 Nov 4.
Lipinski, D.M., Yusuf, M., Barnard, A.R., Damant, C., Issa, P.C., Singh, M.S., Lee, E., Davies, W.L., Volpi, E.V., McLaren, R.E., 2011. Characterization of a dominant cone degeneration in a green fluorescent protein-reporter mouse with disruption of loci associated with human dominant retinal dystrophy. Investig. Ophthalmol. Vis. Sci. 52, 6617–6623.
Münch, T.A., Da Silveira, R.A., Siegert, S., Viney, T.J., Awatramani, G.B., Roska, B., 2009. Approach sensitivity in the retina processed by a multifunctional neural circuit. Nat. Neurosci. 12, 1308–1316.
Nickerson, P.E.B., Ortin-Martinez, A., Wallace, V.A., 2018. Material exchange in photoreceptor transplantation: updating our understanding of donor/host communication and the future of cell engraftment science. Front. Neural Circ. 12, 17.
O'Brien, J.J., Chen, X., Macleish, P.R., O'Brien, J., Massey, S.C., 2012. Photoreceptor coupling mediated by connexin36 in the primate retina. J. Neurosci. 32, 4675–4687.
Ortin-Martinez, A., Yan, N.E., Tsai, E.L.S., Comanita, L., Gurdita, A., Tachibana, N., Liu, Z.C., Lu, S., Dolati, P., Pokrajac, N.T., El-Sehemy, A., Nickerson, P.E.B., Schuurmans, C., Bremner, R., Wallace, V.A., 2021. Photoreceptor nanotubes mediate the in vivo exchange of intracellular material. EMBO J 40 (22), e107264, 2021 Nov 15.
Ovesný, M., Křížek, P., Borkovec, J., Švindrych, Z., Hagen, G.M., 2014. ThunderSTORM: a comprehensive ImageJ plug-in for PALM and STORM data analysis and super-resolution imaging. Bioinformatics 30, 2389–2390.
Pearson, R.A., Barber, A.C., Rizzi, M., Hippert, C., Xue, T., West, E.L., Duran, Y., Smith, A.J., Chuang, J.Z., Azam, S.A., et al., 2012. Restoration of vision after transplantation of photoreceptors. Nature 485, 99–103.
Pearson, R.A., Gonzalez-Cordero, A., West, E.L., Ribeiro, J.R., Aghaizu, N., Goh, D., Sampson, R.D., Georgiadis, A., Waldron, P.V., Duran, Y., et al., 2016. Donor and host photoreceptors engage in material transfer following transplantation of post-mitotic photoreceptor precursors. Nat. Commun. 7, 13029.
Ries, J., Kaplan, C., Platonova, E., Eghlidi, H., Ewers, H., 2012. A simple, versatile method for GFP-based super-resolution microscopy via nanobodies. Nat. Methods 9, 582–584.
Rust, M.J., Bates, M., Zhuang, X., 2006. Sub-diffraction-limit imaging by stochastic optical reconstruction microscopy (STORM). Nat. Methods 3, 793–795.
Santos-Ferreira, T., Postel, K., Stutzki, H., Kurth, T., Zeck, G., Ader, M., 2015. Daylight vision repair by cell transplantation: daylight vision repair by cell transplantation. Stem Cell. 33, 79–90.
Santos-Ferreira, T., Llonch, S., Borsch, O., Postel, K., Haas, J., Ader, M., 2016. Retinal transplantation of photoreceptors results in donor–host cytoplasmic exchange. Nat. Commun. 7, 13028.
Siegert, S., Scherf, B.G., Del Punta, K., Didkovsky, N., Heintz, N., Roska, B., 2009. Genetic address book for retinal cell types. Nat. Neurosci. 12, 1197–1204.
Singh, M.S., Balmer, J., Barnard, A.R., Aslam, S.A., Moralli, D., Green, C.M., Barnea-Cramer, A., Duncan, I., MacLaren, R.E., 2016. Transplanted photoreceptor precursors transfer proteins to host photoreceptors by a mechanism of cytoplasmic fusion. Nat. Commun. 7, 13537.
Solovei, I., Kreysing, M., Lanctôt, C., Kösem, S., Peichl, L., Cremer, T., Guck, J., Joffe, B., 2009. Nuclear architecture of rod photoreceptor cells adapts to vision in mammalian evolution. Cell 137, 356–368.
Swoboda, M., Henig, J., Cheng, H.M., Brugger, D., Haltrich, D., Plumeré, N., Schlierf, M., 2012. Enzymatic oxygen scavenging for photostability without ph drop in single-molecule experiments. ACS Nano 6, 6364–6369.
Szikra, T., Trenholm, S., Drinnenberg, A., Jüttner, J., Raics, Z., Farrow, K., Biel, M., Awatramani, G., Clark, D.A., Sahel, J.A., et al., 2014. Rods in daylight act as relay cells for cone-driven horizontal cell-mediated surround inhibition. Nat. Neurosci. 17, 1728–1735.
Vignais, M.-L., Caicedo, A., Brondello, J.-M., Jorgensen, C., 2017. Cell connections by tunneling nanotubes: effects of mitochondrial trafficking on target cell metabolism, homeostasis, and response to therapy. Stem Cell. Int. 2017, 6917941.